Research Square

Preprints are preliminary reports that have not undergone peer review.
They should not be considered conclusive, used to inform clinical practice,
or referenced by the media as validated information.

Polysorbate 20-Assisted PEG Precipitation for Isolating Sub-100 nm of Turmeric-Derived Exosome-like Nanoparticles with Superior Colloidal Stability

Anitya Shukla
National Institute of Pharmaceutical Education and Research (NIPER-Raebareli) Lucknow (UP)
Nidhi Srivastava
National Institute of Pharmaceutical Education and Research (NIPER-Raebareli) Lucknow (UP)
Niranjan Meher
nmchem.iitg@gmail.com

National Institute of Pharmaceutical Education and Research (NIPER-Raebareli) Lucknow (UP)

Research Article

Keywords: turmeric-derived exosome-like nanoparticles, PEG precipitation, Polysorbate 20, colloidal stability, natural nanocarrier

Posted Date: August 26th, 2026

DOI: https://doi.org/10.21203/rs.3.rs-10702428/v1

License: This work is licensed under a Creative Commons Attribution 4.0 International License.
Read Full License

Additional Declarations: No competing interests reported.

Polysorbate 20-Assisted PEG Precipitation for Isolating Sub-100 nm of Turmeric-Derived Exosome-like Nanoparticles with Superior Colloidal Stability

Anitya Shukla[1], Nidhi Srivastava[*1], Niranjan Meher*[*1]*

[1]Department of Biotechnology, National Institute of Pharmaceutical Education and Research (NIPER-Raebareli) Lucknow (UP)- 226002 (India).

*[1] E-mail: nmchem.iitg@gmail.com; Phone: +91 9078962335

Abstract: Exosomes are nanoscale extracellular vesicles that mediate intercellular communication and are increasingly recognized as versatile bio-nanocarriers for diagnostic and therapeutic applications. Among them, plant-derived exosomes-like nanoparticles from turmeric (*Curcuma longa* L.) offer unique advantages due to their biocompatibility and intrinsic pharmacological activity. However, previously reported extraction methods, such as differential ultracentrifugation or polyethylene glycol (PEG) precipitation at acidic pH, yielded relatively large, polydisperse vesicles (> 180 nm) with limited stability, restricting their translational potential. Herein, we report an optimized PEG precipitation-based protocol integrating Polysorbate 20 (P20) assisted stabilization to isolate turmeric-derived exosome-like nanoparticles (TDEs) with ~100 nm size and markedly improved colloidal stability for up to 15 days. Morphological as well as spectroscopic characterization confirmed the uniform spherical morphology and retention of curcumin-associated molecular features within the vesicles. Stability profiling across pH 5 to 9, ionic solutions, and temperature (4–42 °C) conditions demonstrated robust structural integrity, while repetitive freeze–thaw cycles caused only moderate aggregation. In addition, cell viability analysis demonstrated good biocompatibility of TDEs toward Human Embryonic Kidney Cells (HEK293) over a broad concentration range. The proposed method provides a reproducible, cost-effective, and scalable strategy for isolating functionally stable TDEs, establishing a promising platform for translational drug-delivery and biomedical applications.

Keywords: turmeric-derived exosome-like nanoparticles; PEG precipitation; Polysorbate 20, colloidal stability; natural nanocarrier

Introduction:

Turmeric (*Curcuma longa* L.), a rhizomatous plant of the Zingiberaceae family, has been valued for over centuries in traditional medicine for its diverse pharmacological properties (Prasad & Aggarwal, 2011). Its primary bioactive compound, curcumin, exhibits well-documented antioxidant, anti-inflammatory, antineoplastic, and cardioprotective activities, underpinning its growing biomedical relevance (Maiti & Dunbar, 2018). Recent advances in nanobiotechnology have sparked interest in plant-derived extracellular vesicles (EVs)—particularly exosomes—as natural, biocompatible nanocarriers capable of transporting therapeutic molecules across biological barriers (Jella et al., 2018).

Exosomes, typically ranging from 30 to 150 nm, originate via inward budding of the multivesicular body (MVB) membrane and encapsulate diverse biomolecules such as nucleic acids, proteins, lipids, and metabolites, thereby mirroring the molecular profile of their parent cells (H. Chen et al., 2021; Joshi et al., 2020). Their content reflects cellular physiology and pathophysiology, translating them into powerful tools for biomarker discovery, disease monitoring, and targeted delivery. Notably, elevated exosome secretion has been associated with cancer progression and metastasis, while specific exosomal microRNAs, nucleic acids and proteins have emerged as diagnostic and prognostic biomarkers (Kar et al., 2023; Yu et al., 2025).

Unlike synthetic nanocarriers, exosomes hold significant advantages in next-generation nanocarriers for therapeutic delivery owing to their biocompatibility, low immunogenicity, and intrinsic targeting potential (Simpson et al., 2009). In recent years, plant-derived exosomes (PDEs) have gained attention as sustainable and safe nanocarriers for biomedical applications. The Food and Agriculture Organization (FAO) estimates that more than 50,000 plant species possess therapeutic potential, underscoring the untapped diversity of plant-based bio-nanocarriers (J. Kim et al., 2022). PDEs share several features with mammalian exosomes like size, density, surface charge, and cargo complexity, yet offer unique advantages in extraction, scalability, non-toxicity, and suitability for oral delivery with promising therapeutic efficacy(Mu et al., 2014).

A variety of isolation strategies have been applied to exosome purification, including size-exclusion chromatography, density-gradient separation, differential ultracentrifugation, and polymer-based precipitation, each with intrinsic trade-offs (Gao et al., 2023). Ultracentrifugation, while widely used, requires specialized equipment and may induce shear-

induced damage to vesicle membranes. Density-gradient methods improve purity but are laborious and time-intensive while size-exclusion chromatography maintains vesicle integrity yet provide low yields. In contrast, polyethylene glycol (PEG)-based precipitation offers a simple, scalable, and cost-effective approach without the need for ultrahigh-speed centrifugation (Li et al., 2025). However, PEG methods often result in larger polydisperse vesicles with limited colloidal stability, as demonstrated by *Kumar et al* (Kumar et al., 2024). In our optimized method, Polysorbate 20 (P20) was applied at natural exosomal pH to reduce vesicle size and enhance stability (van de Wakker et al., 2022). These findings highlight the need for refined PEG-based techniques that yield smaller, more stable exosomes suitable for biomedical translation.

In this context, the present study introduces a P20-assisted PEG precipitation protocol for isolating turmeric-derived exosome-like nanoparticles (TDEs) with enhanced physicochemical and colloidal stability. P20, commercially known as Tween 20, a non-ionic surfactant widely recognized for its biocompatibility (van de Wakker et al., 2022), was integrated into the PEG precipitation process to reduce aggregation and promote vesicle dispersion. At concentrations below the critical micelle concentration (CMC), the hydrophobic tail of P20 partially inserts into the phospholipid membrane of exosomes, while the hydrophilic polyoxyethylene chains remain extended into the surrounding aqueous medium. This creates a steric barrier around the vesicles, reducing van-der Waals attraction, nonspecific adsorption, and vesicle-vesicle aggregation, thereby enhancing colloidal stability and a more monodisperse vesicle population without membrane disruption (Pálóczi et al., 2015; Zohouri et al., 2025). The modified method yielded uniform nanoscale TDEs (< 100 nm) with a zeta potential of −35.3 mV and colloidal stability maintained for up to 15 days across diverse media, pH conditions, and temperatures, demonstrating robust structural integrity (**Figure 1**). This represents a significant improvement over previously reported PEG precipitation and ultracentrifugation protocols for isolating TDEs (**Figure 1**) (Kumar et al., 2024). Furthermore, the biocompatibility and cellular response of the isolated TDEs were assessed using an (3-[4,5-dimethylthiazole-2-yl]-2,5-diphenyltetrazolium bromide) MTT assay, which revealed high cell viability, indicating low cytotoxicity and favorable biological compatibility of TDEs (Xu et al., 2019). Moreover, the smaller size range of TDEs (≈30–150 nm) may further enhance their therapeutic potential due to Enhanced Permeability and Retention (EPR) effect, enabling improved tissue penetration, tumor accumulation and cargo delivery in solid tumor possessing dysfunctional vasculature for efficient therapeutic delivery

(Meher et al., 2023).Collectively, these results establish a cost-effective, reproducible, and scalable PEG precipitation strategy for the isolation of TDEs, potentially adaptable to other plant sources, thereby advancing their utility as natural nanocarriers for biomedical and drug-delivery applications.

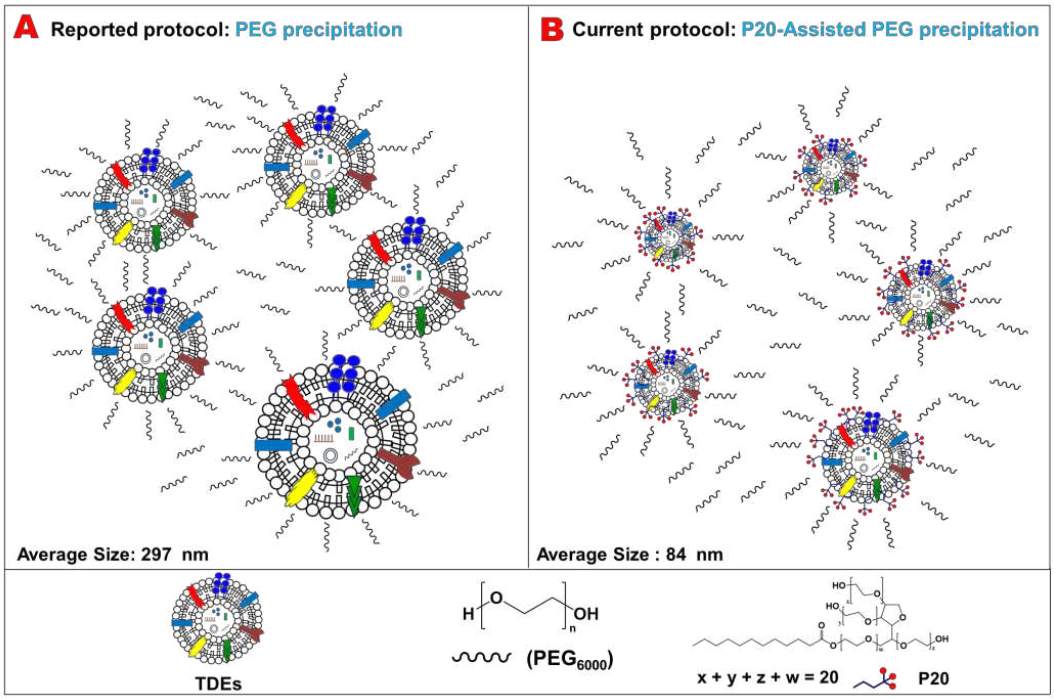


Figure 1. Schematic representation of turmeric-derived exosome-like nanoparticles isolated with or without P20-assisted PEG precipitation technique.

Materials and Methods:

Materials and Instruments: *Curcuma longa* was sourced from the garden at NIPER-Raebareli. RIPA Buffer was purchased from TCI CO. LTD, Folin & Ciocalteu's phenol and Curcumin and Ethanol were purchased from Sigma Aldrich, India. Polyethylene glycol (PEG_{6000}), Sodium Potassium Tartrate, Polysorbate 20 (Tween 20), Na_2CO_3, NaOH, KCl. NaCl, Na_2HPO_4, KH_2PO_4, $CuSO_4.5H_2O$, Bovine serum albumin (BSA), DMEM, RPMI, DMSO, Methanol, fetal bovine serum (FBS), Trypsin, Penicillin-Streptomycin, Citric acid and Sodium-citrate and 3-(4,5-Dimethyl-2-thiazolyl)-2,5-diphenyl-2H-tetrazolium bromide (MTT) were purchased from Himedia. All solvents used were of HPLC grade. High speed cooling centrifuge (ThermoFishcher Scientific: Sorvall ST 8R, Rotor SN. 4760 G), ultracentrifuge (BECKMAN COULTER, Optima xpn-100 Ultracentrifuge, Rotor: 100Ti s/n 20U1638), dynamic light scattering (Malvern Instruments), electron microscope (JEOL JSM-

IT200), atomic force microscope (Park Systems NX12), microplate reader (SYNERGY BioTek, Agilent), FTIR (ALPHA BRUKER), UV-Vis Spectrophotometer (Cary 60 Agilent), HPLC (Agilent 1260 Infinity II), 0.45µ Nylon filter (RanDisc™ Avantor) and ultrapure water (Milli-Q system) was used to in this study.

Authentication of Turmeric Plant: Turmeric plants were collected from the NIPER-Raebareli campus and authenticated based on morphological evaluation of whole, transverse, and longitudinal rhizome sections **(Figure S1).** Further authentication was carried out at the CSIR–National Botanical Research Institute (CSIR-NBRI), Lucknow, India, where a voucher specimen was deposited under Authentication No. PDSH/LWG/Authentication/2025-26/10 **(Figure S2)**.

Isolation and Purification of TDEs: Fresh rhizomes of *Curcuma longa* L. were thoroughly washed with distilled water. The cleaned rhizomes were then finely ground using a sterile mortar and pestle to obtain turmeric juice. The excess fiber was removed by filtration through a nylon mesh (200 µm pore size) to eliminate large debris. The filtrate was subjected to a series of differential centrifugation steps to remove the remaining residual debris. Initially, the extract was centrifuged at 2,000×g for 10 minutes, followed by 6,000×g for 20 minutes at 4 °C to remove large particulates. Subsequently, the supernatant was further centrifuged at 10,000×g for 40 minutes and 12,000×g for 1 hour at 4 °C to eliminate moderate-sized debris. The resulting supernatant was adjusted with 5 mM (3%) PEG_{6000} and the mixture was incubated on a shaker at 4 °C for ~24 hours to facilitate TDEs precipitation. Following incubation, the mixture was centrifuged at 8,000×g for 40 minutes to collect the pellet, which was then resuspended in distilled water containing 0.05 mM P20 for 10 mins. To further purify the TDEs, the suspension was centrifuged again at 12,000×g for 1 hour at 4 °C, and the supernatant was collected and passed through a 0.45 µm syringe filter to remove any remaining impurities. Apart from suspension in distilled water containing 0.05 mM of P20, the pellets were suspended in different media. Such as, ultrapure water, PBS (150 mM), NaCl (154 mM), PBS (150 mM)+NaCl (154 mM), PBS (150 mM)+P20 (0.05 mM), and PBS (150 mM)+NaCl (154 mM)+P20 (0.05 mM) and were centrifuged at the 12000xg followed by 0.45 µm syringe filter to optimize and compare the stability of TDEs in different media. The final TDEs preparation was stored at 4 °C for subsequent studies.

Dynamic Light Scattering (DLS): The hydrodynamic diameter, size distribution and zeta potential of TDEs were analyzed in triplicates at 1 mg/mL concentration under the following

conditions: backscattering angle 173° and equilibrium time 120 s (Malvern Zetasizer). Additionally, the colloidal behavior of TDEs (0.1 mg/mL) was analyzed using DLS and zeta potential to determine changes in size, PDI and ZP under various environmental conditions (pH, temperature, buffers, etc.) up to 3-15 days by incubating at 4 ^{o}C and were subjected to 20 seconds of gentle vortexing before data acquisition.

Morphological Analysis: Scanning Electron Microscopy (SEM) images were recorded in a JEOL JSM-IT200, where the purified TDEs were lyophilized to dry and dispersed over aluminum foil surface followed by gold coating. The images were acquired at an acceleration voltage of 15 kV.

The morphological analysis of TDEs was also done using High-resolution Transmission Electron Microscopy (HR-TEM, Talos, F200X G2 TEM, USA). 10 µl of the extracted TDEs (1 mg/mL) was diluted in 1 ml of ultrapure water. Now, 10 µl the sample was drop-casted on a carbon-coated copper grid stained with 2% uranyl acetate in dark for 2 min, then dried in vacuum and images were recorded.

Atomic Force Microscopy (AFM) characterization was conducted using a Park Systems NX12 in non-contact mode with an NCHR cantilever. 10 µl of the sample (1 mg/mL) was drop-casted on a mica sheet, air-dried at room temperature, and three dimensional images were recorded. Using the software XEI, the particle size and roughness parameters were analysed.

Ultraviolet-Visible (UV-Vis) Spectroscopy: The spectra were recorded to evaluate the optical absorption profiles of TDEs using UV–Visible spectrophotometer and were compared with commercially available curcumin. Briefly, UV-Visible spectra of 5 µg/mL each of the TDEs and curcumin were recorded in methanol (99.9%), solvents, along with their mixture in the range of 300–600 nm.

HPLC-Based Quantification of Curcumin: TDEs membranes were lysed using methanol to release and solubilize curcumin present within or associated with the lipid bilayer prior to quantification (Ambarsari et al., 2026)(Wei et al., 2023). Curcumin quantification was performed using high-performance liquid chromatography (HPLC). Chromatographic analysis was carried out using a C18 column (4.6 mm × 250 mm, 5 µm particle sizes). The mobile phase consisted of acetonitrile (ACN) and 4% glacial acetic acid (GAA) solution in a 9:1 ratio, delivered at a flow rate of 0.6 mL/min. The column temperature was maintained at

25 °C and detection was performed at 425 nm with an injection volume of 10 µL. The curcumin content was determined to be ≈ 4 µg per mg of exosomal protein, corresponding to 0.4% (w/w) relative to protein.

Fourier Transform Infrared Spectroscopy (FT-IR): FT-IR spectra of curcumin, turmeric powder, and TDEs were recorded and compared to examine the functional groups and chemical bonds present in the samples. For analysis, 1–2 mg of each dried sample was directly placed on the sample holder, and spectra were recorded in the range of 4000–400 cm^{-1} with a resolution of 4 cm^{-1}, averaging 16 scans per sample. The characteristic absorption bands corresponding to –OH, C=O, C–H, polar head of lipids and aromatic rings were analyzed and compared across the three samples to evaluate their chemical composition and potential similarities.

Protein quantification and analysis: Protein concentration was estimated using the standard Lowry method. Briefly, 20 µL aliquot of the protein sample (with or without RIPA buffer) was added to each well, followed by 125 µL of Reagent C, prepared by mixing Reagent A (2% Na_2CO_3 in 0.1 N NaOH) with Reagent B (0.5% $CuSO_4$ in 1% sodium potassium tartrate). The mixture was incubated for 10 min at room temperature. The intensity of this color, measured spectrophotometrically at 660 nm, is proportional to the protein content. A standard curve prepared with BSA was used to calculate the protein concentration of the samples (Li et al., 2016).

Colloidal Stability Study: The colloidal stability of TDEs was systematically evaluated under varying biological media, pH, temperature, and freeze–thaw conditions to assess their physicochemical robustness by monitoring the variation in their hydrodynamic diameter (DLS), surface charge (zeta potential), and/or protein content (Lowry Assay). For stability in bio-relevant media study, TDEs suspensions (1 mg/mL) were incubated in 150 mM phosphate-buffered saline (PBS, pH 7.4), 154 mM sodium chloride (NaCl), Dulbecco's Modified Eagle Medium (DMEM), RPMI-1640 and Fetal Bovine Serum (FBS) at 4 °C. The samples were monitored over a 15-day period. For pH-dependent stability, TDEs suspensions were adjusted to pH 5.0, 7.4, or 9.0 using 0.1 M HCl or NaOH and incubated at 4 °C and monitored for 72 h. Temperature stability was assessed by incubating aliquots at 4 °C, 25 °C, 37 °C, and 42 °C for 72 h. After incubation, samples were equilibrated to room temperature before analysis. For freeze–thaw stress testing, TDEs samples were subjected to three consecutive freezing and thawing (−20 °C and −80 °C to RT, 30 min/cycle) cycles.

Cell Viability Assay: HEK293 cells used in this project were procured from the repository of the National Centre for Cell Science (NCCS) Pune, India. The cells were proliferated to confluence in Dulbecco's modified Eagle's medium (DMEM, Sigma) supplemented 10% FBS and 1% penicillin/streptomycin, and maintained at 37 °C in a 5% CO_2 incubator. HEK293 cells were seeded in a 96-well cell culture plate at a density of 1×10^4 cells/well and incubated overnight at 37 °C in a 5% CO_2 incubator. The cells were treated with different concentrations of TDEs (0-400 µg/mL) for 24 h. After completion of the treatment for 24 h, the growth medium was removed and washed, and 50 µL of MTT solution (0.5 mg/mL) was added in each well and again incubated for 3h. Cell viabilities were determined by reading the absorbance of the wells at 570 nm with a microplate reader post dissolving the formazan crystal in DMSO for 30 minutes.

Statistical Analysis: All studies were performed in triplicate (n = 3), and results are presented as mean ± standard deviation (SD). Data analysis was performed using GraphPad Prism (version 8.0.1 (244)) and OriginPro (version 2025b) software. One-way and two-way analysis of variance (ANOVA) among multiple groups was performed for statistical comparisons. A p-value < 0.05 was considered statistically significant.

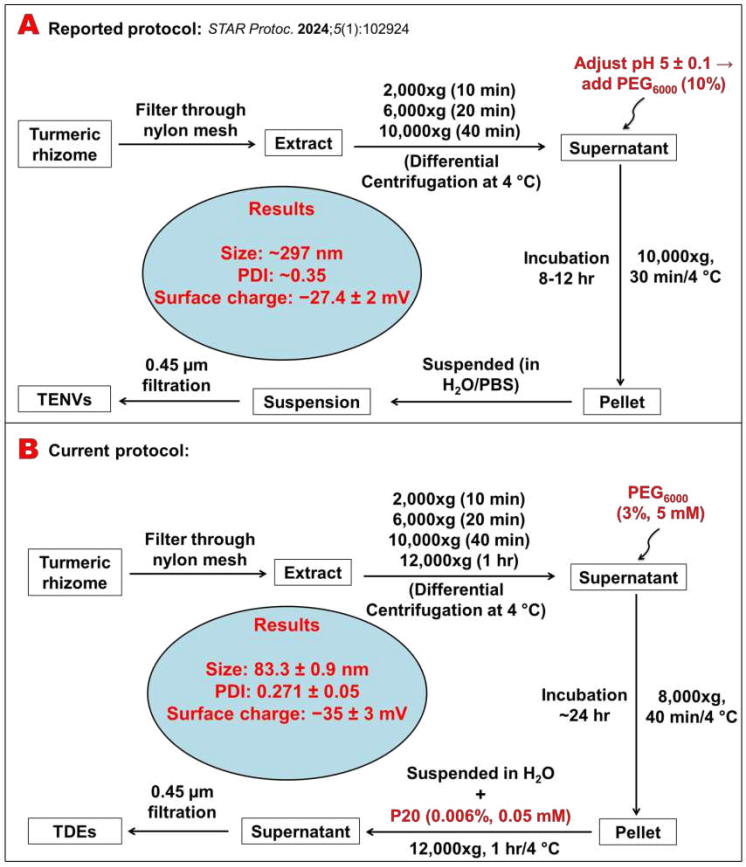


Figure 2. Comparative schematic representation of TDEs isolations. Previously reported **(A)** versus current **(B)** protocol for TDEs isolation using PEG precipitation technique.

Results and Discussion:

Optimization of TDEs Isolation Protocol: It is of continuous challenge to isolate smaller size, preferably ~100 nm, TDEs with improved colloidal stability, which is of utmost requirement to achieve better drug delivery and therapeutic efficacy *in vivo*. **Figure 2A** schematically present the detail protocol reported previously for the isolation of TDEs using PEG precipitation technique, where the supernatant after differential centrifugation has been adjusted to pH 5 in the presence of 10% PEG (Kumar et al., 2024). Although the protocol improved TDEs yield by maintaining acidic pH condition, it produced relatively larger size (~297 nm) extracellular vesicles with poor colloidal stability. Similarly, another report with 8-15 % of PEG_{6000} yielded extracellular vesicles from ginger with size ~252 nm or more (Kalarikkal et al., 2020). Herein, a simple yet strategic modification of PEG precipitation protocol has been developed, optimized, and validated to obtain stable, nanosized (~100 nm) TDEs by integrating P20 as a stabilizing agent. As depicted in **Figure 2B**, the key modification in the current technique is the use of 3% PEG_{6000} instead of 10%, and the

subsequent suspension of pellet in aqueous solution containing 0.006% P20. The optimized approach produced vesicles with average hydrodynamic diameter of 82.13 nm and zeta potential of −35.3 mV, confirming uniform size distribution and excellent colloidal stability (**Figure S3**)(Midekessa et al., 2020a). These findings confirm that P20 integration enhances vesicle dispersion and stability compared with previously reported PEG precipitation along with ultracentrifugation (UC) methods (Kumar et al., 2024)(Wei et al., 2023). Further, to have a direct comparison with the PEG precipitation method, TDEs were isolated by following the previously reported gold-standard ultracentrifugation based isolation protocol (Wei et al., 2023). TDEs isolated via PEG precipitation showed an average hydrodynamic diameter of 102.75 nm, whereas UC-isolated TDEs exhibited a size of 130 nm or larger with comparable surface charge **(Figure S4A-C, Table S1)**. Protein quantification further revealed higher protein recovery in PEG precipitation-derived TDEs, with concentrations of 305.16 µg/mL without RIPA and 490 µg/mL with RIPA, compared to 176.56 µg/mL without RIPA and 418.88 µg/mL with RIPA for UC-isolated TDEs **(Figure S4D, Table S1)**, which could be due to its efficient precipitation of vesicles with minimal structural stress in PEG precipitation method (Huang et al., 2025). In contrast, repeated high-speed centrifugation during UC may contribute to partial exosomal loss through vesicle deformation, aggregation, or incomplete pellet recovery (T. Kim et al., 2025). Collectively, these findings indicate superior exosomal yield with favorable physicochemical characteristics via the PEG precipitation method.

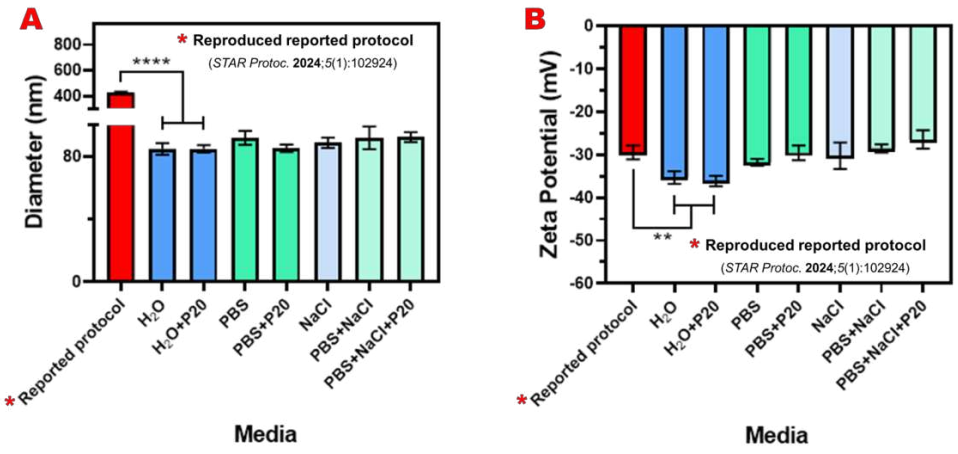


Figure 3. Effect of buffer treatments on TDEs isolation. Hydrodynamic diameter **(A)** and surface charge analysis **(B)** measured after resuspension of the isolated TDEs in different

medium on Day 0 of isolation: *Reproduced reported protocol (Kumar et al., 2024), H_2O, H_2O+P20, PBS, PBS+P20, NaCl, PBS+NaCl and PBS+NaCl+P20. (n=3, Mean ± SD)

Effect of Suspension Media and Comparison with Reported PEG Precipitation Protocol: The size distribution and homogeneity of the isolated TDEs were observed in different suspension media. DLS measurement study showed that the resuspension of the pellet in different media (H_2O, H_2O+P20, PBS, PBS+P20, NaCl, PBS+NaCl, PBS+NaCl+P20) yielded highly homogenous TDEs in the range of 84.86 ± 3.03 to 92.44 ± 2.54 nm size (**Figure 3A, S5-S10, Table S2**). For a direct comparison with earlier studies, TDEs were also isolated in-house using the previously reported PEG precipitation protocol performed at pH 5.0 without P20. The resulting vesicles exhibited an average hydrodynamic diameter of 423.1 ± 9.51 nm and zeta potential of −29.4 ± 1.30 mV (**Figure S11, Table S2**), values that were comparable to the prior literature, thereby validating the reproducibility of earlier PEG-based isolation approaches under acidic conditions. Interestingly, the P20-assisted PEG precipitation protocol yielded significantly smaller TDEs as compared to the commonly used ultracentrifugation techniques (> 200 nm) as well (Wei et al., 2023). Zeta potential analysis revealed that TDEs suspended in H_2O or H_2O+P20 medium exhibited a slightly higher negative surface charge (< −35 mV) compared to those dispersed in ionic media such as NaCl or PBS (−30.2 ± 2.53 to −31.7 ± 0.62 mV) on day 0 of isolation (**Figure 3B, S3, S5-S12**). This reduction in zeta potential in ionic medium could be due to slight increase in particle proximity that promotes TDEs aggregation and relative size enlargement (Midekessa et al., 2020b).

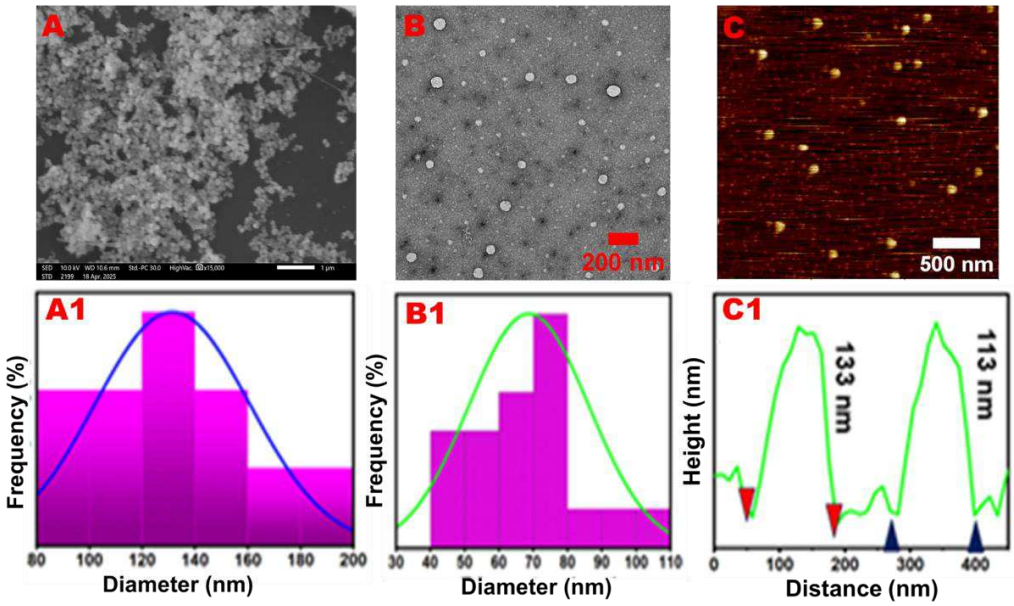


Figure 4. Microscopic analysis of TDEs. Scanning electron microscopic (**A**), Transmission electron microscopic (**B**) and Non-contact atomic force microscopic image (**C**) of TDEs with corresponding size distributions (**A1-C1**). TDEs were resuspended in water and drop-casted followed by drying for TEM and AFM analysis, whereas the lyophilized TDEs were imaged for SEM analysis.

Morphological Characterization: The morphology and structural integrity of the isolated TDEs were analyzed using SEM, TEM, and AFM (**Figure 4**). SEM imaging of lyophilized TDEs demonstrated spherical to slightly oval vesicles (100–150 nm) with smooth surfaces (**Figure 4A, A1**). High-resolution TEM images confirmed spherical to slightly oval morphology with diameters of 70–80 nm (**Figure 4B, B1**), consistent with DLS data. AFM topography showed round, evenly distributed vesicles with low surface roughness (**Figure 4C, C1**), indicating morphological uniformity. Furthermore, as a negative control, P20 at 4 mM (0.5%) concentration was subjected to DLS analysis demonstrating the formation of micelles of below 20 nm size, which is in agreement of the prior report (**Figure S13A,B)** (Basheva et al., 2007). In contrast, SEM, TEM and AFM micrographs showed vesicles of ~100 nm, consistent with the characteristic size of TDEs, suggesting that the observed vesicles were TDEs rather than P20 micelles (Basheva et al., 2007). Collectively, these complementary techniques confirm that the TDEs were sub-100 nm sized, structurally stable, and aggregation-free, validating the efficiency of the modified isolation protocol (Raimondo et al., 2015).

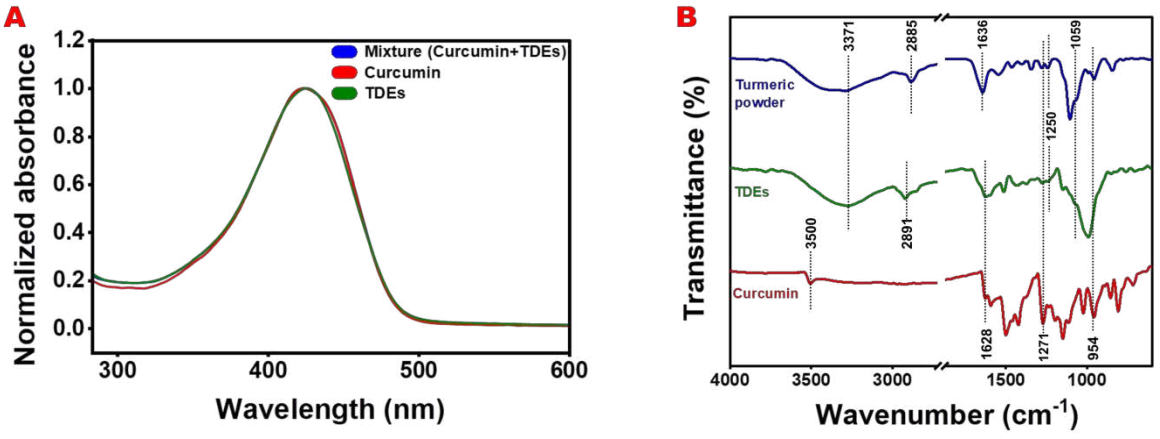


Figure 5. UV-Vis and FT-IR spectra of TDEs. Normalized UV-Vis Absorption Spectra of TDEs, Curcumin, and mixture (Curcumin + TDEs) **(A)** and FT-IR spectra of TDEs, Curcumin, and Turmeric powder **(B).**

Spectroscopic Characterization: UV–Vis spectroscopy confirmed the presence of curcumin-associated chromophores within TDEs. Pure curcumin exhibited a broader band (420–435 nm) with $\lambda_{abs.max}$ at 425nm, corresponding to π–π* transitions of its conjugated system. The curcumin standard as well as mixture of curcumin and TDEs displayed similar bands, superimposable when normalized, with $\lambda_{abs.max}$ at 425 and 425 nm respectively, indicating curcumin incorporation in the TDEs (**Figure 5A and S14**) (Yuyama et al., 2012; Zhang et al., 2016).

Furthermore, HPLC analysis confirmed the presence of curcumin in TDEs. **Figure S15** illustrates the calibration curve of curcumin, while **Figure S16A-B** presents the HPLC chromatograms of standard curcumin and TDEs, showing retention times of 4.75 min and 4.8 min, respectively, thereby confirming the presence of curcumin-associated compounds within the TDEs. Quantitative analysis further demonstrated that the curcumin content in TDEs was approximately 1.6 µg/mL corresponding to 0.4% w/w (Kumar et al., 2024; Nanoparticles et al., 2023).

FT-IR analysis confirmed the presence of multiple similar characteristic functional groups in curcumin, TDEs, and turmeric powder, indicating their structural similarity. Curcumin displayed peaks at 3500 cm^{-1} (O–H stretching), 1628 cm^{-1} (C=C and C=O stretching), 1271 cm^{-1} (enolic C–O), and 954 cm^{-1} (aromatic trans-CH), confirming its polyphenolic nature (Singh et al., 2014)(X. Chen et al., 2015). TDEs showed similar curcumin-associated peaks at 1628, 1271 and 954 cm^{-1} along with additional bands at 1059 cm^{-1} (C–O–C stretching), 3371 cm^{-1} (amide A), 1250 cm^{-1} (amide III), and 2891 cm^{-1} (lipid head groups, the CH_2 stretching vibrations), consistent with their lipid–protein membrane composition (Ji et al., 2020). Besides, turmeric powder exhibited corresponding peaks related to curcumin and lipid components. Collectively, FT-IR analyses substantiated the structural and biochemical resemblance among curcumin, TDEs, and turmeric powder **(Figure 5B).**

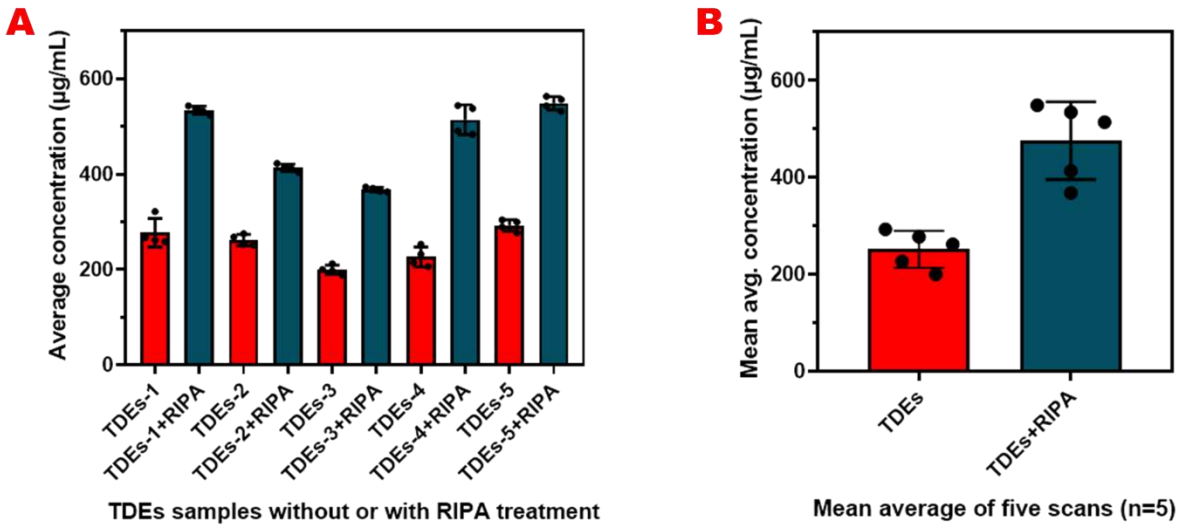


Figure 6. Proteins quantification in TDEs. Quantification of protein content in the isolated TDEs from 5 different batches **(A),** and respective mean average concentration **(B)** following Lowry colorimetric assay. (n=5, Mean ± SD)

Protein Quantification: Protein content of the TDEs were estimated following the standard Lowry colorimetric assay after extracting the vesicles with and without radioimmunoprecipitation assay (RIPA) buffer, which is a cell lysis buffer used to extract and solubilize proteins from cells and tissues (Frostadottir et al., 2025). The protein content was calculated to be 475.39 ± 71.80 µg/mL (with RIPA) and 251.45 ± 33.95 µg/mL (without RIPA), indicating successful isolation of vesicle-associated proteins **(Figure 6A,B, S17, Table S3,S4)**. These values are highly comparable with the previously reported TDEs protein levels across different plant source and extraction technique (Assink Junior et al., 2023). Proteins form the functional core of TDEs, and protein richness in the vesicles validates their biological relevance (Tóth et al., 2021).

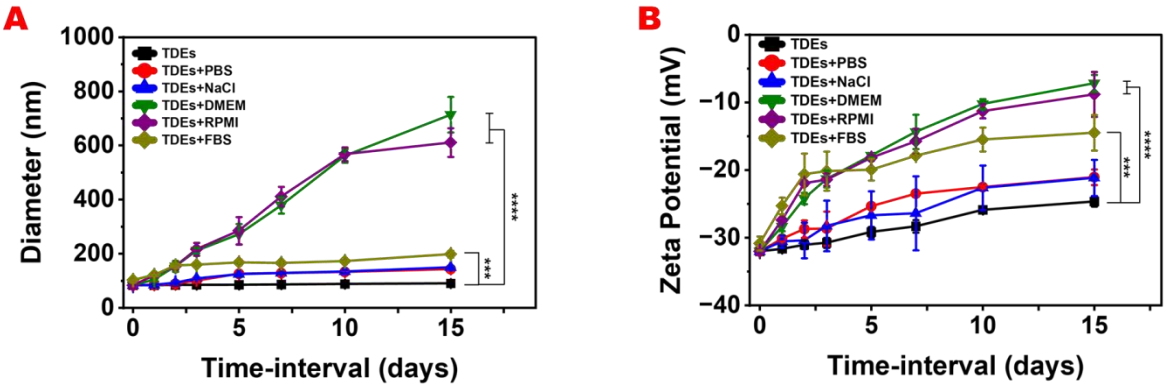


Figure 7. Effect of different media on the stability of TDEs. Hydrodynamic diameter **(A)** and surface charge analysis **(B)** of TDEs suspended in 150 mM PBS, 154 mM NaCl, RPMI, DMEM and FBS (50%) media. The samples were incubated at 4 ºC and data were acquired at RT. (n=3, Mean ± SD)

Colloidal Stability in Bio-relevant Media: To assess environmental stability, TDEs were dispersed in PBS (150 mM), NaCl (154 mM), DMEM, RPMI-1640 and FBS, followed by 15-day DLS monitoring **(Figure 7A,B, S18, Table S5,S6)**. Native TDEs exhibited a hydrodynamic diameter of 83.25 ± 0.87 nm, and surface charge -32.33 ± 0.3 mV, increasing modestly over time to 90.4 ± 0.52 nm, and surface charge -24.6 ± 0.7 mV, demonstrating good stability. In PBS and NaCl, the vesicles maintained a hydrodynamic diameter in the range of 142.9 ± 11.6-149.63 ± 4.95 nm, and surface charge in the range of -21.06 ± 1.15 to -21.16 ± 2.67 mV, increasing slightly to that of native TDEs (-24.6 ± 0.7 mV) up to day 15, which may be due to salt accumulation on the vesicle membranes. However, no visible aggregation was observed, demonstrating preserved integrity under physiological ionic conditions. Conversely, TDEs in DMEM and RPMI induced significant growth in size (up to 713.26 ± 65.69 nm and 610.7 ± 52.8 nm, respectively) and increased zeta potential (-7.2 ± 1.2 to -8.8 ± 3.3 mV), indicating instability likely due to protein corona formation around TDEs due to electrostatic interactions and protein aggregation (**Figure 7A,B, Table S5-S6**) (Wei et al., 2023; Yuyama et al., 2012; Zhang et al., 2016). Furthermore, TDEs incubated in 1%, 10%, and 50% FBS media exhibited a time- and concentration-dependent increase in hydrodynamic diameter, and zeta potential over 15 days, indicating reduced colloidal stability at higher FBS concentrations. The particle size increased from an initial 102.75 nm to 198.46 nm in 50% FBS, while zeta potential shifted from -31.7 mV to -14.5 mV at 50% FBS media, respectively **(Figure S19A-C, Table S7)**. Among the tested conditions, TDEs suspended in 1% FBS exhibited comparatively lower physicochemical changes, whereas higher serum concentrations resulted in pronounced aggregation and reduced stability (Santos et al., 2023; Tóth et al., 2021). Collectively, isotonic salts preserved TDEs physicochemical stability, while nutrient-rich culture media and higher serum concentrations compromised colloidal integrity, highlighting the critical influence of medium composition on TDEs stability (Li et al., 2016).

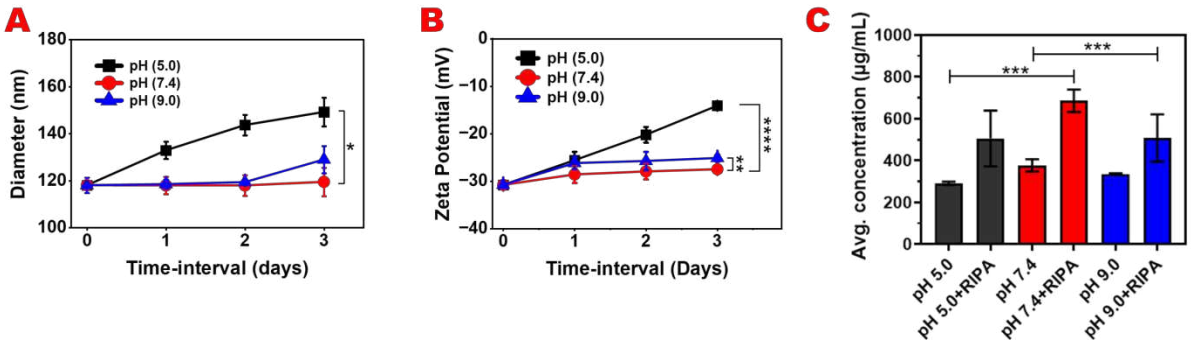


Figure 8. Effect of pH variation on TDEs characterization. Hydrodynamic diameter **(A)**, surface charge analysis **(B)** and average protein concentrations **(C)** of TDEs at three different pH values i.e. 5.0, 7.4 and 9.0. The samples were incubated at 4 °C and data were acquired at RT (n=3, Mean ± SD).

Effect of pH on Stability:

The freshly isolated TDE suspension exhibited a pH of 6.8 ± 0.1. Although extracellular vesicles do not possess an intrinsic pH, this value represents the pH of the TDEs suspension under our isolation conditions and may contribute to its physicochemical characteristics and colloidal stability. TDEs were incubated at different pH of 5.0, 7.4, and 9.0 (by adjusted using 0.1 M HCl/NaOH) to evaluate their stability over 3 days (**Figure 8A–C, S20, Table S8**). At pH 7.4 and 9.0, vesicles showed hydrodynamic diameter in the range of 118.33 ± 3.3 to 128.93 ± 5.7 nm, and surface charge –27.5 ± 0.86 to –25.13 ± 0.75 mV, which were very comparable with the native TDEs demonstrating relatively stable colloidal systems. Under acidic conditions (pH 5.0), size and surface charge increased noticeably to 149.2±6.07 nm and –14.1 ± 0.69 mV respectively (**Figure 8B**). This change might be attributed to protonation of surface groups, leading to reduced electrostatic repulsion and membrane destabilization (Midekessa et al., 2020b).

Protein quantification revealed the highest levels (376.67 ± 24.10 µg/mL without RIPA and 685.17 ± 43.67 µg/mL with RIPA) at physiological pH 7.4, whereas both acidic and basic conditions resulted in reduction in the protein content of the TDEs **(Table S9)**, likely due to membrane leakage and cytosolic release (Cheng et al., 2019). These findings confirm that pH variations modulate TDEs protein retention by altering surface charge and integrity, with physiological pH favoring maximal stability (Larson et al., 2022; Patel et al., 2021).

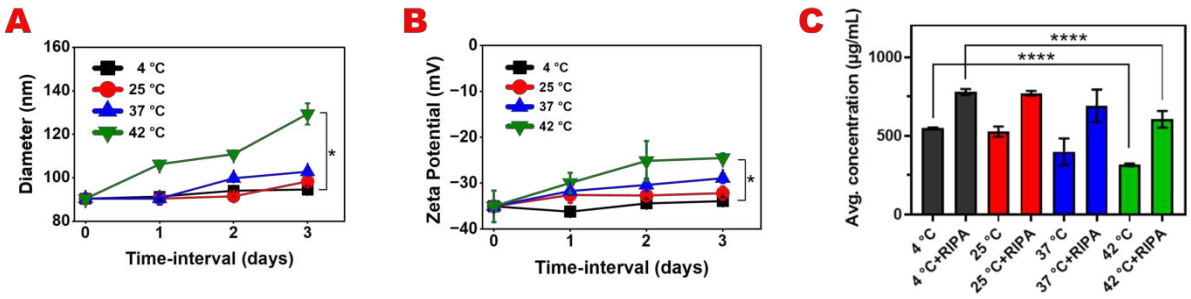


Figure 9. Effect of different temperature on TDEs characterization. Hydrodynamic diameter **(A)**, Surface charge **(B)** and Protein content **(C)** of TDEs at four different temperatures i.e. 4 °C, 25 °C, 37 °C and 42 °C, monitored over 3 days (n=3, Mean ± SD).

Temperature-Dependent Behavior: The temperature stability of the TDEs were evaluated at four different temperatures i.e. 4 °C, 25 °C, 37 °C and 42 °C, over 3 days in which day 0 was measured before the treatment. The size of the TDEs remain very stable (< 100 nm) at temperature 37 °C or below, whereas their size increased slightly to 129.3 ± 4.8 nm at 42 °C, indicating partial aggregation **(Figure 9A, S21, Table S10)**. The zeta potential increased steadily (from –35.07 ± 3.4 to –24.53 ± 1.01 mV), whereas protein content reduced steadily (from 549.93 ± 1.3 to 314.94 ± 6.5 µg/mL without RIPA, from 778.67 ± 14.9 to 604.32 ± 43.2 µg/mL with RIPA) with increase in incubation temperature from 4 °C to 42 °C, over 3 days **(Figure 9B,C, Table S10)**. The observed change in surface charge and protein content in TDEs **(Table S11)** indicated heat-induced lipid fusion, membrane fluidity and protein denaturation with increase in temperature (Cheng et al., 2019; Lehman et al., 2023; Takakura et al., 2024). Despite these changes, no visible precipitation occurred, suggesting moderate thermal resilience.

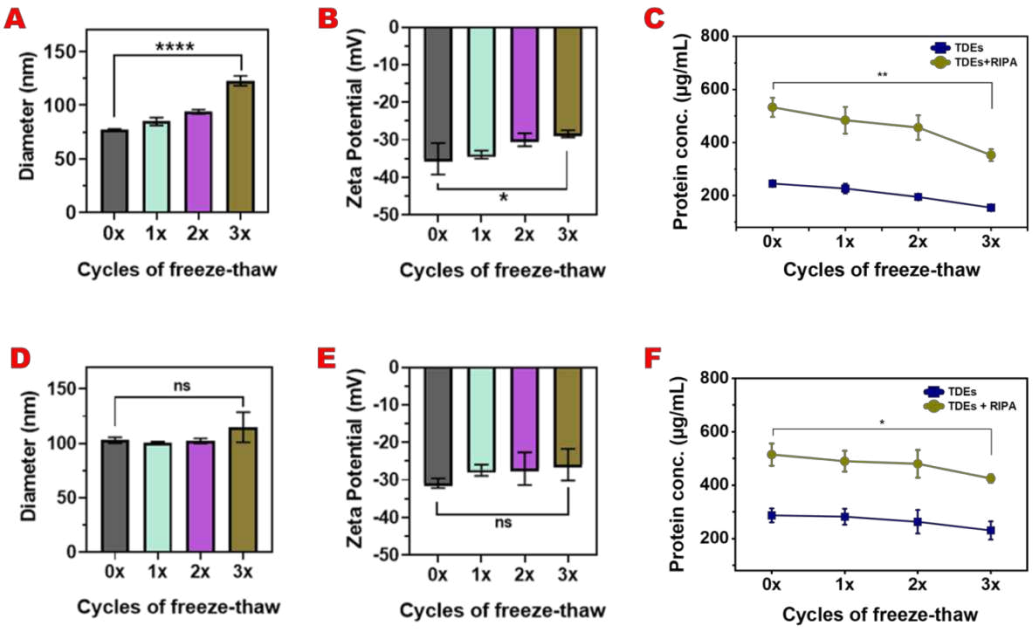


Figure 10. Effect of freeze–thaw cycles on TDEs stability. Hydrodynamic diameter, surface charge, and protein content of TDEs during freeze–thaw cycles at –20 °C to RT (A–C) and –80 °C to RT (D-F) (n = 3, Mean ± SD).

Freeze–Thaw Stability: Three consecutive cycle of freeze-thaw stress tests (-20 °C ↔ RT, 3 cycles and -80 °C ↔ RT, 3 cycles) were performed to evaluate the physical stability of the TDEs (**Figure 10A–F, S22A,B, Table S12**). Initially, the TDEs exhibited an average hydrodynamic diameter of 77.21 ± 0.5nm, a PDI of 0.283 ± 0.004, and a surface charge of -35.07 ± 3.4 mV, which increased gradually to 122.8 ± 3.7 nm, 0.40 ± 0.34, and –28.43 ± 0.78 mV, respectively, post three freeze–thaw cycles. In contrast, TDEs stored at −80 ºC showed relatively lower changes, with hydrodynamic diameter increasing from 102.75 ± 2.1 nm to 114.75 ± 11.2 nm, and surface charge from −30.86 ± 1.04 mV to −25.9 ± 3.4 mV following three cycles. Protein concentration also declined progressively at both storage conditions; however, the reduction was more pronounced at −20 ºC, decreasing from 245.24 ± 10.9 to 154.45 ± 12.4 µg/mL without RIPA and from 532.85 ± 36.8 to 352.78 ± 22.1 µg/mL with RIPA, whereas at −80 ºC it decreased from 286.68 ± 26.07 to 230.14 ± 34.19 µg/mL without RIPA and from 514.42 ± 41.69 to 424.81 ± 15.35 µg/mL with RIPA. Overall, the performed freeze-thaw stress tests indicate partial vesicle fusion and gradual loss of homogeneity in TDEs because of membrane disruption and leakage of internal cargo (Lehman et al., 2023). However, these findings also suggest that TDEs are moderately stable under limited freeze-thaw conditions; however, repeated cycles compromise their structural and functional integrity, which could be overcome by employing suitable cryoprotectants (Park et al., 2018).

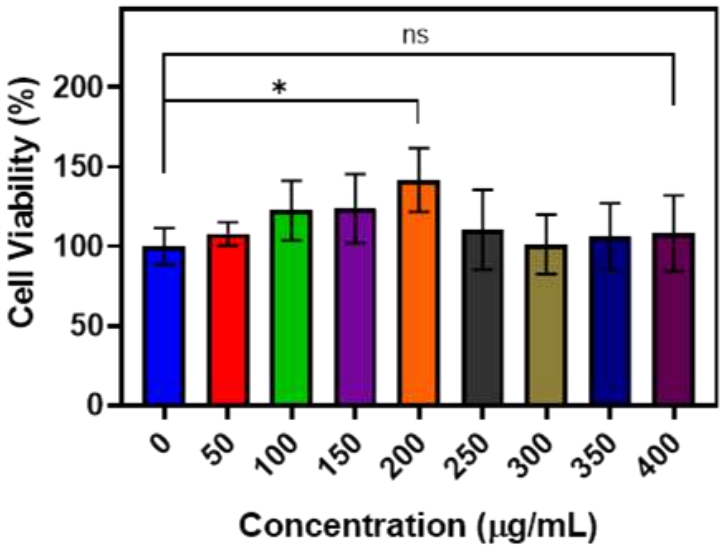


Figure 11. Effect of different concentrations of TDEs on HEK293 cells viability assessed by MTT assay after treatment with 0-400 µg/mL TDEs. Data are presented as mean (n = 3, Mean ± SD).

Cell Viability Assay: The cytocompatibility of TDEs was evaluated in HEK293 cells using the MTT assay over a concentration range of 0–400 µg/mL **(Figure 11, Table S13)**. TDEs exhibited high biocompatibility at lower and intermediate concentrations, with cell viability remaining above 100%, indicating enhanced cellular metabolic activity and negligible cytotoxicity. The highest cell viability was observed at 200 µg/mL, suggesting a possible proliferative or cytoprotective effect of TDEs on HEK293 cells. Overall, the results demonstrated good cell viability over a broad concentration range, indicating that the isolated TDEs stabilized by using the P20 are biocompatible and do not exhibit significant cytotoxic effects under the tested conditions, which could be attributed to the use very low concentration of P20 (0.006%, ~0.05 mM), well below its critical micelle concentration (CMC) (Hock et al., 2017; Xu et al., 2019).

Conclusion: In this study, we successfully modified and evaluated the PEG precipitation protocol for the isolation of TDEs with enhanced colloidal and physicochemical stability by integrating P20 as a stabilizer. The modified approach yielded uniform vesicles below 100 nm, substantially smaller and more monodisperse than those obtained via previously reported PEG precipitation and ultracentrifugation methods. Systematic stability evaluation across different bio-relevant media, pH, temperature, and multiple freeze-thaw cycles demonstrated that the TDEs remained structurally and functionally stable under physiological and moderate

stress conditions. Comprehensive morphological and spectroscopic analyses (SEM, TEM, AFM, UV–Vis, FT-IR and HPLC) verified structural integrity, spherical geometry, and retention of associated bioactive components. These results not only establish the robustness of P20-assisted PEG precipitation for scalable TDEs production but also potential cost-effective method to extract naturally derived nanocarriers for biomedical and therapeutic applications. Besides, cell viability assay demonstrated that TDEs exhibited good biocompatibility toward HEK293 cells across a broad concentration range. Further studies are underway to explore the TDEs as a natural nanocarrier suitable for biomedical and drug-delivery applications.

Acknowledgments:

The authors acknowledge financial support from the Department of Science and Technology (DST), India (NM, DST/INSPIRE/04/2022/001608), Anusandhan National Research Foundation, India (NM, ANRF/ARG/2025/000585/LS; NS, ANRF/ARG/2025/000590/LS); and Department of Pharmaceuticals (Chemicals and Fertilizers, Govt. of India). The authors thank the Central Instrument Facility, National Institute of Pharmaceutical Research and Education, Raebareli (NIPER-R) for instrument and infrastructure facility.

Corresponding Authors Information

Dr. Nidhi Srivastava

*E-mail: nidhi.niperr@gmail.com

ORCID: 0000-0003-3410-4855

Dr. Niranjan Meher

*E-mail: nmchem.iitg@gmail.com

ORCID: 0000-0003-3558-371

Supporting information

Supporting information (SI) is provided and available: S1-S17 and Table S1-S10

Data availability:

All the data relevant to this work have been uploaded as the supporting information file.

Statements and Declarations

Competing interest: There are no any competing interest of authors to declare.

References:

Ambarsari, C. G., Martinez-jarquin, S., Koh, J. J. R., Needham, G., Arkill, K. P., James, V., Taal, M. W., Kim, J. J., Kim, H., & Piccinini, A. M. (2026). *Analytical Methods Optimised untargeted metabolomics work fl ow for human urinary extracellular vesicles* 18:2748–2764. https://doi.org/10.1039/d6ay00002a

Assink Junior, E. J., de Jesus, P. C., & Borges, E. M. (2023). Whey Protein Analysis Using the Lowry Assay and 96-Well-Plate Digital Images Acquired Using Smartphones. *Journal of Chemical Education* 100:2329–2338. https://doi.org/10.1021/acs.jchemed.2c00830

Basheva, E. S., Kralchevsky, P. A., & Danov, K. D. (2007). *The colloid structural forces as a tool for particle characterization and control of dispersion stability w* 3:1308–1317. https://doi.org/10.1039/b705758j

Chen, H., Wang, L., Zeng, X., Schwarz, H., Nanda, H. S., Peng, X., & Zhou, Y. (2021). Exosomes, a New Star for Targeted Delivery. *Frontiers in Cell and Developmental Biology* 9:751079. https://doi.org/10.3389/fcell.2021.751079

Chen, X., Zou, L., Niu, J., Liu, W., Peng, S., & Liu, C. (2015). *The Stability, Sustained Release and Cellular Antioxidant Activity of Curcumin Nanoliposomes* 20:14293–14311. https://doi.org/10.3390/molecules200814293

Cheng, Y., Zeng, Q., Han, Q., & Xia, W. (2019). Effect of pH, temperature and freezing-thawing on quantity changes and cellular uptake of exosomes. *Protein and Cell* 10:295–299. https://doi.org/10.1007/s13238-018-0529-4

Frostadottir, D., Welinder, C., Perez, R., & Dahlin, L. B. (2025). *Refinement of Protein Extraction Protocols for Human Peripheral Nerve Tissue*. *ACS Omega* 10:5111–5118. https://doi.org/10.1021/acsomega.4c11373

Gao, J., Li, A., Hu, J., Feng, L., Liu, L., & Shen, Z. (2023). Recent developments in isolating methods for exosomes. *Frontiers in Bioengineering and Biotechnology* 10:1–17. https://doi.org/10.3389/fbioe.2022.1100892

Hock, A., Miyake, H., Li, B., Lee, C., Ermini, L., Koike, Y., Chen, Y., Määttänen, P., Zani, A., & Pierro, A. (2017). *Breast milk-derived exosomes promote intestinal epithelial cell*

growth 52:755–759. https://doi.org/10.1016/j.jpedsurg.2017.01.032

Huang, Q., Wang, J., Ning, H., Liu, W., & Han, X. (2025). *Exosome isolation based on polyethylene glycol (PEG): a review*. Bioanalysis 17:2847–2861. https://doi: 10.1007/s11010-024-05191-x.

Jella, K. K., Nasti, T. H., Li, Z., Malla, S. R., Buchwald, Z. S., & Khan, M. K. (2018). Exosomes, Their Biogenesis and Role in Inter-Cellular Communication, Tumor Microenvironment and Cancer Immunotherapy. *Vaccines* 6:69. https://doi.org/10.3390/vaccines6040069

Ji, Y., Yang, X., Ji, Z., Zhu, L., Ma, N., Chen, D., Jia, X., Tang, J., & Cao, Y. (2020). DFT-Calculated IR Spectrum Amide I, II, and III Band Contributions of N-Methylacetamide Fine Components. *ACS Omega* 5:8572–8578. https://doi.org/10.1021/acsomega.9b04421

Joshi, B. S., de Beer, M. A., Giepmans, B. N. G., & Zuhorn, I. S. (2020). Endocytosis of Extracellular Vesicles and Release of Their Cargo from Endosomes. *ACS Nano* 14:4444–4455 https://doi.org/10.1021/acsnano.9b10033

Kalarikkal, S. P., Prasad, D., Kasiappan, R., Chaudhari, S. R., & Sundaram, G. M. (2020). A cost-effective polyethylene glycol-based method for the isolation of functional edible nanoparticles from ginger rhizomes. *Scientific Reports* 10:4456. https://doi.org/10.1038/s41598-020-61358-8

Kar, R., Dhar, R., Mukherjee, S., Nag, S., Gorai, S., Mukerjee, N., Mukherjee, D., Vatsa, R., Chandrakanth Jadhav, M., Ghosh, A., Devi, A., Krishnan, A., & Thorat, N. D. (2023). Exosome-Based Smart Drug Delivery Tool for Cancer Theranostics. *ACS Biomaterials Science & Engineering* 9:577–594. https://doi.org/10.1021/acsbiomaterials.2c01329

Kim, J., Li, S., Zhang, S., & Wang, J. (2022). Plant-derived exosome-like nanoparticles and their therapeutic activities. *Asian Journal of Pharmaceutical Sciences* 17:53–69. https://doi.org/10.1016/j.ajps.2021.05.006

Kim, T., Hong, J. W., Lee, L. P., & Lee, L. P. (2025). *Efficient methods of isolation and purification of extracellular vesicles*. Nano Converg. 12:64. doi: 10.1186/s40580-025-00523-z.

Kumar, M. N., Kalarikkal, S. P., Jayaram, Y., Narayanan, J., & Sundaram, G. M. (2024). Protocol to produce plant-based hybrid nanovesicles from fresh turmeric and pepper using polyethylene glycol. *STAR Protocols* 5:102924. https://doi.org/10.1016/j.xpro.2024.102924

Larson, N. R., Hu, G., Wei, Y., Tuesca, A. D., Forrest, M. L., & Middaugh, C. R. (2022). pH-Dependent Phase Behavior and Stability of Cationic Lipid-mRNA Nanoparticles. *Journal of Pharmaceutical Sciences* 111:690–698. https://doi.org/10.1016/j.xphs.2021.11.004

Lehman, S. E., Benkstein, K. D., Cleveland, T. E., Anderson, K. W., Carrier, M. J., & Vreeland, W. N. (2023). Particle Metrology Approach to Understanding How Storage Conditions Affect Long-Term Liposome Stability. *Langmuir* 39:12313–12323. https://doi.org/10.1021/acs.langmuir.3c01270

Li, L., Piontek, K. B., Kumbhari, V., Ishida, M., & Selaru, F. M. (2016). Isolation and Profiling of MicroRNA-containing Exosomes from Human Bile. *Journal of Visualized Experiments : JoVE* 112:54036. https://doi.org/10.3791/54036

Li, L., Zheng, Z., Lan, W., Tang, N., Zhang, D., Ling, J., Wu, Y., Yang, P., Fu, L., Liu, J., Zhang, J., Yu, P., & Huang, T. (2025). Role of Exosomes in Cardiovascular Disease: A Key Regulator of Intercellular Communication in Cardiomyocytes. *ACS Omega* 10:18145–18169. https://doi.org/10.1021/acsomega.4c11423

Maiti, P., & Dunbar, G. L. (2018). Use of Curcumin, a Natural Polyphenol for Targeting Molecular Pathways in Treating Age-Related Neurodegenerative Diseases. *International Journal of Molecular Sciences* 19:1637. https://doi.org/10.3390/ijms19061637

Meher, N., Vanbrocklin, H. F., & Wilson, D. M. (2023). *PSMA-Targeted Nanotheranostics for Imaging and Radiotherapy of Prostate Cancer*. Pharmaceuticals (Basel) 16:315. https://doi: 10.3390/ph16020315.

Midekessa, G., Godakumara, K., Ord, J., Viil, J., Lättekivi, F., Dissanayake, K., Kopanchuk, S., Rinken, A., Andronowska, A., Bhattacharjee, S., Rinken, T., & Fazeli, A. (2020a). Zeta Potential of Extracellular Vesicles: Toward Understanding the Attributes that Determine Colloidal Stability. *ACS Omega* 5:16701–16710.

https://doi.org/10.1021/acsomega.0c01582

Midekessa, G., Godakumara, K., Ord, J., Viil, J., Lättekivi, F., Dissanayake, K., Kopanchuk, S., Rinken, A., Andronowska, A., Bhattacharjee, S., Rinken, T., & Fazeli, A. (2020b). Zeta Potential of Extracellular Vesicles: Toward Understanding the Attributes that Determine Colloidal Stability. *ACS Omega* 5:16701–16710. https://doi.org/10.1021/acsomega.0c01582

Mu, J., Zhuang, X., Wang, Q., Jiang, H., Deng, Z.-B., Wang, B., Zhang, L., Kakar, S., Jun, Y., Miller, D., & Zhang, H.-G. (2014). Interspecies communication between plant and mouse gut host cells through edible plant derived exosome-like nanoparticles. *Molecular Nutrition & Food Research* 58:1561–1573. https://doi.org/10.1002/mnfr.201300729

Wei Y, Cai X, Wu Q, Liao H, Liang S, Fu H, et al (2023) Extraction, isolation, and component analysis of turmeric-derived exosome-like nanoparticles. Bioengineering (Basel) 10:1147. https://doi.org/10.3390/bioengineering10101147

Pálóczi, K., Vukman, K. V, Tamási, V., Balogh, A., & Kittel, Á. (2015). *Biomolecular Chemistry vesicle subpopulations* 13:9775–9782. https://doi.org/10.1039/c5ob01451d

Park, S., Jeon, H., Yoo, S.-M., & Lee, M.-S. (2018). The effect of storage temperature on the biological activity of extracellular vesicles for the complement system. *In Vitro Cellular & Developmental Biology - Animal* 54:423–429. https://doi.org/10.1007/s11626-018-0261-7

Patel, P., Ibrahim, N. M., & Cheng, K. (2021). The Importance of Apparent pKa in the Development of Nanoparticles Encapsulating siRNA and mRNA. *Trends in Pharmacological Sciences* 42:448–460. https://doi.org/10.1016/j.tips.2021.03.002

Prasad, S., & Aggarwal, B. B. (2011). *Turmeric, the Golden Spice: From Traditional Medicine to Modern Medicine.* In: Benzie IFF, Wachtel-Galor S (eds) Herbal medicine: biomolecular and clinical aspects, 2nd edn. Boca Raton Taylor & Francis, pp 261–284

Raimondo, S., Naselli, F., Fontana, S., Monteleone, F., Lo Dico, A., Saieva, L., Zito, G., Flugy, A., Manno, M., Di Bella, M. A., De Leo, G., & Alessandro, R. (2015). Citrus limon-derived nanovesicles inhibit cancer cell proliferation and suppress CML xenograft growth by inducing TRAIL-mediated cell death. *Oncotarget* 6:19514–19527.

https://doi.org/10.18632/oncotarget.4004

Santos, L. M., Cardoso, P. S., Diniz, E. A., Rahhal, J. G., & Sipert, C. R. (2023). Different concentrations of fetal bovine serum affect cytokine modulation in lipopolysaccharide-activated apical papilla cells in vitro. J Appl Oral Sci 31:20230020. https://doi.org/10.1590/1678-7757-2023-0020.

Simpson, R. J., Lim, J. W. E., Moritz, R. L., & Mathivanan, S. (2009). Exosomes: proteomic insights and diagnostic potential. *Expert Review of Proteomics* 6:267–283. https://doi.org/10.1586/epr.09.17

Singh, P., Wani, K., Kaul-Ghanekar, R., Prabhune, A., & Ogale, S. (2014). From micron to nano-curcumin by sophorolipid co-processing: Highly enhanced bioavailability, fluorescence, and anti-cancer efficacy. *RSC Adv.* 4:59601–59611. https://doi.org/10.1039/C4RA07300B

Takakura, Y., Hanayama, R., Akiyoshi, K., Futaki, S., Hida, K., Ichiki, T., Ishii-Watabe, A., Kuroda, M., Maki, K., Miura, Y., Okada, Y., Seo, N., Takeuchi, T., Yamaguchi, T., & Yoshioka, Y. (2024). Quality and Safety Considerations for Therapeutic Products Based on Extracellular Vesicles. *Pharmaceutical Research* 41:1573–1594. https://doi.org/10.1007/s11095-024-03757-4

Tóth, E. Á., Turiák, L., Visnovitz, T., Cserép, C., Mázló, A., Sódar, B. W., Försönits, A. I., Petővári, G., Sebestyén, A., Komlósi, Z., Drahos, L., Kittel, Á., Nagy, G., Bácsi, A., Dénes, Á., Gho, Y. S., Szabó-Taylor, K. É., & Buzás, E. I. (2021). Formation of a protein corona on the surface of extracellular vesicles in blood plasma. *Journal of Extracellular Vesicles* 10:12140. https://doi.org/10.1002/jev2.12140

van de Wakker, S. I., van Oudheusden, J., Mol, E. A., Roefs, M. T., Zheng, W., Görgens, A., El Andaloussi, S., Sluijter, J. P. G., & Vader, P. (2022). Influence of short term storage conditions, concentration methods and excipients on extracellular vesicle recovery and function. *European Journal of Pharmaceutics and Biopharmaceutics* 170:59–69. https://doi.org/10.1016/j.ejpb.2021.11.012

Xu, F., Xiang, Q., Huang, J., Chen, Q., Yu, N., Long, X., & Zhou, Z. (2019). *Exosomal miR-423-5p mediates the proangiogenic activity of human adipose- derived stem cells by targeting Sufu* 10:106. https://doi.org/10.1186/s13287-019-1206-3.

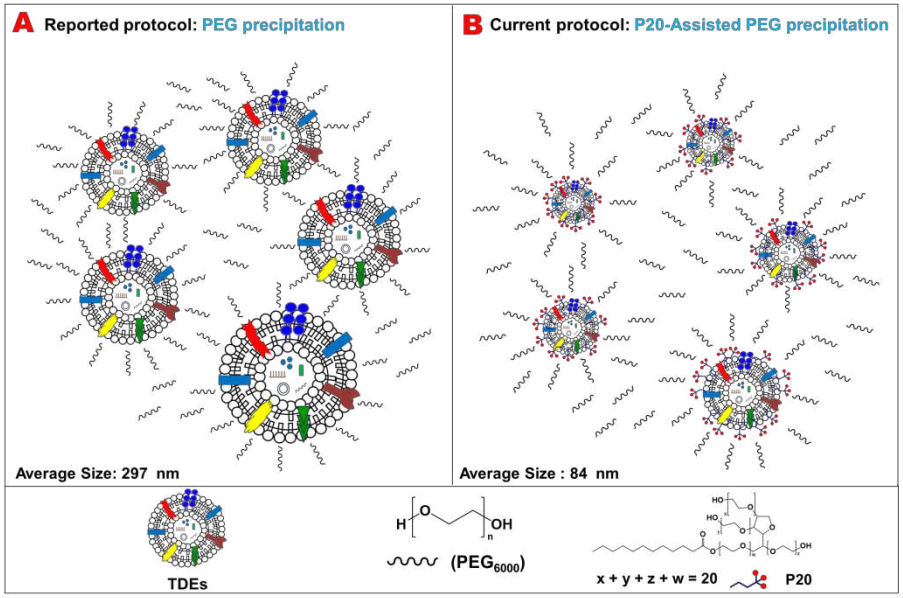
Yu, J., Zhou, R., Liu, S., Zheng, J., Yan, H., Su, S., Chai, N., Segal, E., Jiang, C., Guo, K., & Li, C. (2025). Electrochemical Biosensors for the Detection of Exosomal microRNA Biomarkers for Early Diagnosis of Neurodegenerative Diseases. *Analytical Chemistry* 97:5355–5371. https://doi.org/10.1021/acs.analchem.4c02619

Yuyama, K., Sun, H., Mitsutake, S., & Igarashi, Y. (2012). Sphingolipid-modulated exosome secretion promotes clearance of amyloid-β by microglia. *The Journal of Biological Chemistry* 287:10977–10989. https://doi.org/10.1074/jbc.M111.324616

Zhang, Z., Leong, D. J., Xu, L., He, Z., Wang, A., Navati, M., Kim, S. J., Hirsh, D. M., Hardin, J. A., Cobelli, N. J., Friedman, J. M., & Sun, H. B. (2016). Curcumin slows osteoarthritis progression and relieves osteoarthritis-associated pain symptoms in a post-traumatic osteoarthritis mouse model. *Arthritis Research & Therapy* 18:128. https://doi.org/10.1186/s13075-016-1025-y

Zohouri, D., Duc, T., Reyre, M., Smadja, C., Krupova, Z., Talbot, L., & Taverna, M. (2025). Talanta Elucidation of extracellular vesicles behavior during capillary isoelectric focusing. *Talanta* 293:128055. https://doi.org/10.1016/j.talanta.2025.128055

TOC



Polysorbate 20–assisted PEG precipitation enables the facile isolation of uniform, sub-100 nm turmeric-derived exosome-like nanoparticles with markedly enhanced colloidal stability and structural integrity.

Supplementary Files

This is a list of supplementary files associated with this preprint. Click to download.

- SITDEs13082026.docx